Optics Communications 426 (2018) 182–186

Contents lists available at ScienceDirect

Optics Communications

journal homepage: www.elsevier.com/locate/optcom

Compact static birefringent spectral range enhanced Fourier transform imaging spectrometer

Jie Li [a,*], Haiying Wu [b], Chun Qi [a]

[a] Department of Information and Communication Engineering, School of Electronic and Information Engineering, Xi'an Jiaotong University, Xi'an 710049, China
[b] Huayin Ordnance Test Center, Huayin 710042, China

ARTICLE INFO

Keywords:
Imaging spectrometer
Fourier transform
Spectral range enhanced
Birefringence

ABSTRACT

A compact static birefringent spectral range enhanced Fourier transform imaging spectrometer (SEFTIS) is presented. The key component of the proposed SEFTIS is a new static dual-path birefringent interferometer formed by a polarizer, a Wollaston prism and a modified Glan–Taylor prism. Without any moving elements, it produces two independent interference patterns for two wavebands detections simultaneously, thereby providing at least twice the width of the original working spectral range. Compared with previous spectral range enhanced imaging spectrometers, the developed sensor highly reduces the complexity and alignment difficulty of the system. Theory and experimental prototype working in 400–1700 nm are described in detail.

1. Introduction

Imaging spectrometer is often designed to measure the spatial image and spectral composition of an object. It has become a well-recognized technique in many fields, including astronomy, environment monitoring, biomedical medicine, and other scientific and industrial areas, as a powerful tool for objects detection and identification with preferable accuracy [1–6]. As to a spectral device, its performance is quantified by the following critical parameters: spectral range (detectable wavelength range), spectral resolution and signal to noise ratio (SNR). To satisfy a variety of application requirements, the spectral range must be large and the spectral resolution and SNR must be fine [7]. However, the spectral range of a system is not only restricted by the responding range of the focal plane array (FPA), but also by the optical efficiency of the spectroscopic components. Conventional method to solve this problem is employing multiple subsystems. Each subsystem is an independent spectral imaging device enable to acquire data covering a portion of the spectral range [8]. In this way, the weight, volume and cost will highly increased. Additionally, considerable care is required for field of view registration. Another approach has been a multichannel configuration with beam splitters, separated dispersive optics (interferometers) and FPAs, which share a common aperture and field of view for every channel [9,10]. The drawbacks are the complexity, alignment difficulty and optical efficiency loss.

In this paper, we propose a novel birefringent spectral range enhanced Fourier transform imaging spectrometer (SEFTIS). The configuration employs a polarizer, a Wollaston prism and a modified Glan–Taylor prism to produce two interferograms for two wavebands detections simultaneously. For a demonstration, a 400–1700 nm spectral range enhanced system based on this configuration is presented. We show that the described model blends the advantage of a grating spectrometer and a Michelson interferometer: extremely compact, robust, and wide free spectral range.

2. Theory

2.1. System structure

The optical schematic of the developed SEFTIS is illustrated in Fig. 1. It consists of a fore-optics, a slit, a collimator, a polarizer P, a Wollaston prism WP, a modified Glan–Taylor prism MGP, two imaging lenses, and two FPAs (InGaAs and CCD).

Light from the object is collected and collimated by fore-optics and collimator, and then incidents on P. The light emerging from P becomes linearly polarized at 45° to the optic axes of the Wollaston prism. WP split the incoming light into two orthogonally polarized components, extraordinary ray e and ordinary ray o, with equal amplitudes and a small divergent angle. Note that here the polarization orientations of e ray and o ray are 45° and −45° to the x axis, respectively. After passing through MGP, the two component rays are resolved into four linearly polarized rays. The two transmitted rays (oe, ee) and two reflected rays (eo, oo) have same polarization orientation separately and launched into

* Corresponding author.
E-mail address: jielixjtu@xjtu.edu.cn (J. Li).

https://doi.org/10.1016/j.optcom.2018.05.045
Received 19 February 2018; Received in revised form 8 April 2018; Accepted 13 May 2018

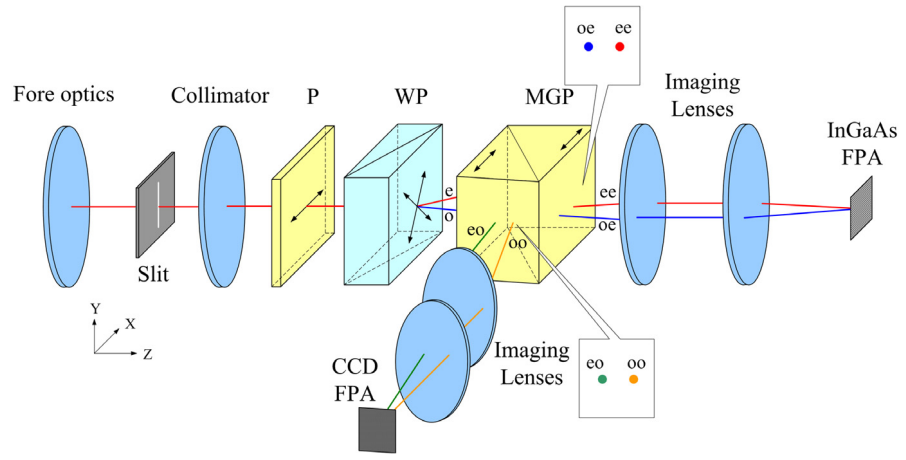

Fig. 1. Schematic of the developed static dual-path birefringent interferometer. The optic axes of the polarization elements are indicated by arrows.

two FPAs. The interferograms are thus created on the focal plane of the imaging lenses. The CCD and InGaAs FPA then record the visible–near infrared (VIS–NIR, 400–1000 nm) and near infrared (NIR, 900–1700 nm) interferogram patterns along the row dimension and spatial imaging (1D) of the object along the column dimension simultaneously. Another spatial dimension is derived by scanning the system across the object. This is the so-called "push-broom" data acquisition mode. This kind of data acquisition mode makes the result instrument very suitable for working on a moving platform (e.g. airplane, UAV), since the instrument has not any mechanical moving parts and the scanning can be derived from the motion of the platform.

2.2. Modified Glan–Taylor prism

MGP is the key element of the proposed interferometer, as shown in Fig. 2. It is combined by two calcite crystal wedge plates with their principle sections parallel to each other. The left plate is an isosceles triangle with the structure angle θ which ensures the identical incident angle and emergent angle. There is an air gap between the left and right wedge plate. Due to the birefringence of calcite, incident light is resolved into two orthogonally linearly polarized rays in the left plate, one ordinary and one extraordinary. The structure angle θ is set about 39.6°. Since the ordinary refractive index n_o is bigger than extraordinary one n_e, total internal reflection of the ordinary ray will occur at the air gap while the extraordinary ray will pass through the right wedge plate. The MGP designed here is employed as an analyzer to obtain two sets of coherent light with same vibration direction. It can also acts as a beam splitter to produce two interference channels for two working wavebands.

2.3. Operation principle

The functional form of the two interferogram can be described as [11,12]:

$$I_{Vis-Nir}(\delta) = I_{V0} - 2t_1t_2\int_{\sigma_1}^{\sigma_2} S_{Vis-Nir}(\sigma)\cos(2\pi\delta\sigma)\,d\sigma, \tag{1}$$

and

$$I_{Nir}(\delta) = I_{N0} + 2t_1t_3\int_{\sigma_3}^{\sigma_4} S_{Nir}(\sigma)\cos(2\pi\delta\sigma)\,d\sigma \tag{2}$$

where I_{V0} and I_{N0} are bias terms. δ is the optical path difference (OPD) introduced by the WP; t_1 is the transmittance of the polarizer P; t_2 and t_3 characterize the o ray and e ray transmittances of MGP, respectively; $S_{Vis-Nir}(\sigma)$ and $S_{Nir}(\sigma)$ are the spectra of the object point in VIS–NIR and NIR band, respectively; $\sigma = 1/\lambda$ is the wavenumber. Note that since the transmission axes of P and MGP are crossed in the VIS–NIR band and co-aligned in the NIR band, the signs of the second terms in Eqs. (1) and (2) are negative and positive, respectively.

The OPD introduced by WP is [13]

$$\delta_{Vis-Nir} = 2B(\sigma)x\tan(\alpha)/M_V, \tag{3}$$

and

$$\delta_{Nir} = 2B(\sigma)x\tan(\alpha)/M_N. \tag{4}$$

Here $B(\sigma) = n_e(\sigma) - n_o(\sigma)$ is the birefringence of the crystal; α is the wedge angle of WP; M_V and M_N are the magnifications of the imaging lenses of two bands, respectively; x is the displacement of the fringe line from the zero OPD point on the FPA. The parameters $B(\sigma)$, M_V, M_N and α are fixed when the system is built up. δ only varies with x along one-dimension of the FPA. Thus, when light from an object point incident into the system, the spectra can be obtained by performing the inverse Fourier transform [11]

$$\begin{aligned} S_{Vis-Nir}(\sigma) &= \Im^{-1}\left\{I_{Vis-Nir}(x) - I_{V0}\right\} \\ &= \int_{-\infty}^{+\infty}(I_{Vis-Nir}(x) - I_{V0}) \\ &\quad \times \exp(-i4\pi\sigma B(\sigma)\tan(\alpha)/M_V)dx, \end{aligned} \tag{5}$$

and

$$\begin{aligned} S_{Nir}(\sigma) &= \Im^{-1}\left\{I_{Nir}(x) - I_{N0}\right\} \\ &= \int_{-\infty}^{+\infty}[I_{Nir}(x) - I_{N0}]\exp(-i4\pi\sigma B(\sigma)\tan(\alpha)/M_N)dx. \end{aligned} \tag{6}$$

Here the proportionality constants have been dropped, since the shapes of the spectra would not be affected by them.

The spectral resolutions of the two wavebands for unapodized interferograms are [11]:

$$\Delta\sigma_{Vis-Nir} = \frac{1}{2\delta_{Vis-Nir}}, \tag{7}$$

$$\Delta\sigma_{Nir} = \frac{1}{2\delta_{Nir}}. \tag{8}$$

It should be indicated that the maximum spectral resolution is not only determined by the OPD of the WP, but also affected by the sampling numbers of the CCD and InGaAs FPA. The maximum spectral resolutions are given by [14]

$$\Delta\sigma_{\max Vis-Nir} = \frac{2}{N_{Vis-Nir}\cdot\lambda_{\min Vis-Nir}}, \tag{9}$$

$$\Delta\sigma_{\max Nir} = \frac{2}{N_{Nir}\cdot\lambda_{\min Nir}}. \tag{10}$$